Ferromagnetic quantum criticality in the alloy CePd1−xRhx

J. G. Sereni, T. Westerkamp, R. Küchler, N. Caroca-Canales, Philipp Gegenwart, C. Geibel

Ferromagnetic quantum criticality in the alloy CePd$_{1-x}$Rh$_x$

J. G. Sereni,[1] T. Westerkamp,[2] R. Küchler,[2] N. Caroca-Canales,[2] P. Gegenwart,[2] and C. Geibel[2]

[1]*Division Bajas Temperaturas, Centro Atómico Bariloche, 8400 San Carlos de Bariloche, Argentina*
[2]*Max-Planck Institute for Chemical Physics of Solids, D-01187 Dresden, Germany*

The CePd$_{1-x}$Rh$_x$ alloy exhibits a continuous evolution from ferromagnetism (T_C=6.5 K) at x=0 to a mixed-valence (MV) state at x=1. We have performed a detailed investigation on the suppression of the ferromagnetic (F) phase in this alloy using dc (χ_{dc}) and ac (χ_{ac}) susceptibility, specific heat (C_m), resistivity (ρ), and thermal expansion (β) techniques. Our results show a continuous decrease of $T_C(x)$ with negative curvature down to T_C=3 K at x^*=0.65, where a positive curvature takes over. Beyond x^*, a cusp in χ_{ac} is traced down to T_C^*=25 mK at x=0.87, locating the critical concentration between x=0.87 and 0.90. The quantum criticality of this region is recognized by the $-\log(T/T_0)$ dependence of C_m/T, which transforms into a T^{-q} ($q \approx 0.5$) one at x=0.87. At high temperature, this system shows the onset of valence instability revealed by a deviation from Vegard's law (at $x_V \approx 0.75$) and increasing hybridization effects on high-temperature χ_{dc} and $\rho(T)$. Coincidentally, a Fermi liquid contribution to the specific heat (γ) arises from the MV component, which becomes dominant at the CeRh limit. In contrast to antiferromagnetic systems, no C_m/T flattening is observed for $x > x_{cr}$ but, rather, the mentioned power-law divergence, which coincides with a change of sign of $\beta(T)$. The coexistence of F and MV components and the sudden changes in the T dependencies are discussed in the context of randomly distributed magnetic and Kondo couplings.

I. INTRODUCTION

The physics related to magnetic critical points at very low temperatures, where quantum fluctuations compete with classical thermal fluctuations, is a topic of increasing interest. The wealthy spectrum of recently discovered properties has triggered intense experimental and theoretical activity, involving a large number of magnetic phase diagrams.[1] The magnetic phase boundaries of those systems are tuned to different classes of critical points,[2–4] where the long-range order is suppressed by applying pressure or by alloying. Since most of the current investigations are devoted to antiferromagnetic (AF) systems, suitable candidates for the study of ferromagnetic (F) systems remain scarce.[5] These systems are different not only in the number of available exemplary AF or F systems, but also in the intrinsic physical properties such as those observed in $3d$ compounds[6] or those proposed by theoretical models.[7] To date, a large number of AF systems exhibiting a coexistence of the magnetic order and the Kondo effect with respect to the number of F ones remain a puzzling problem. This asymmetry cannot be simply explained by a distribution of Ce-Ce spacings in their respective lattices, where intersite magnetic interactions (J_R) occur, mediated by the Ruderman-Kittu-Kasuya-Yoshida mechanism. In spite of that, it is observed that F-Ce binary compounds only appear within a narrow Ce-Ce spacing range: $3.7 < d_{Ce-Ce} < 4.1$ Å.[8] Furthermore, coincident with the fact that the Kondo effect is related to an AF spin-electron-coupling parameter (J_K), none of the known F-Ce compounds show conclusive indications of significant hybridization effects or heavy-fermion behavior. Consequently, the F-order is generally taken as a sign of trivalent Ce^{3+} ground state[5,8] when it reaches the expected entropy ($S_m = R \ln 2$) at $T \approx T_C$.

The few known F-Ce phase diagrams studied as a function of pressure [e.g., CeRu$_2$Ge$_2$,[9] CePd$_2$Al$_2$Ga,[10] and CePt

(Ref.[11])] also show some peculiarities. To our knowledge, none of them show superconductivity, whereas the $T_C(p)$ phase boundary shows the characteristic maximum described by the Doniach-Lavagna model.[12] Under alloying, other intrinsic differences between F and AF systems concerning their respective "final" (nonmagnetic) ground states (GS) are observed. Whereas the former systematically exhibit a *mixed-valence* (MV) state, the latter show a *heavy-fermion* (HF) behavior.[13] Such a difference indicates that a strong hybridization (even including charge fluctuations) is required to overcome a F-GS, whereas in AF spin fluctuations (with $T_K \simeq 10$ K) are enough to screen Ce magnetic moments.[13,14]

The distinctive features between F and AF systems suggest intrinsic differences in their critical points. In fact, theory predicts that they differ in magnetic, thermal, and transport properties.[7] In compounds tuned by pressure, the F-GS is believed to end in a first-order transition, disappearing at a classical critical point (CP) at finite temperatures. On the contrary, some disorder introduced by alloying could smear out the first-order phase transition, resulting in a continuous disappearance of the magnetic order.[15] These predictions make F-alloys particularly interesting for the study of F-CP.

Among F-Ce compounds driven to a nonmagnetic state by doping Ce-ligands, the binary CePd$_{1-x}$Rh$_x$ is one of the most suitable for this study. This system evolves from a F-Ce^{3+} state with T_C=6.6 K to a nonmagnetic MV, with susceptibility (χ_{dc}) and electrical resistivity (ρ) maxima at $T \approx 280$ K.[16] Its cell volume decreases continuously with x, showing a deviation from Vegard's law around x_V=0.75, while L_{III} x-ray absorption spectroscopy (XAS) measurements[16] indicate a significant decrease of the $4f$ state occupancy beyond that concentration. Early studies[17] have extrapolated $T_C(x)$ → 0 from $T > 3$ K at $x \approx 0.65$. However, recent investigations performed at lower temperature revealed that $T_C(x)$ does not

tend to zero at the previously reported value because its negative curvature changes to slightly positive at $x^* \approx 0.63$. Consequently, the $T_C \rightarrow 0$ extrapolation was indeed found at $x_{cr} \approx 0.85$.[18] Since the lowest transition temperature was observed at $T_C(x=0.80)=0.25$ K, CePd$_{1-x}$Rh$_x$ became one of the few systems in which the phase boundary was traced within more than one decade[19] and became the only ferromagnetic one. These properties make CePd$_{1-x}$Rh$_x$ an ideal candidate for the study of F-quantum CP.

II. EXPERIMENTAL DETAILS AND RESULTS

A series of nine samples was prepared in the range of $0.6 \leqslant x \leqslant 1$ by arc melting the appropriate amount of pure elements under argon atmosphere. In order to ensure homogeneity, the resulting buttons were flipped over and remelted several times. For a further improvement of the homogeneity, the buttons were melted again in a high-frequency levitation crucible. At the end of this process, the mass loss was found to be negligible (generally below 0.1%). The samples were then annealed for 7 days at 700 °C in dynamic vacuum. Powder XR diffraction of crushed samples confirmed the orthorhombic CrB structure[20] and did not reveal signs of secondary phases. Since the Bragg peaks of the as crushed samples were rather broad, the powder used for the XR measurements was annealed at 700 °C for 24 h. in dynamic vacuum, leading to much narrower peaks. Using these sharp diffraction patterns, we could determine precise values of the lattice parameters.

A standard superconducting quantum interference device magnetometer was used for the determination of the magnetization from 2 K up to room temperature in a 0.1 T magnetic field. The ac susceptibility was measured using the mutual inductance technique, with a lock-in amplifier as detector working between 0.1 and 12.8 kHz with an excitation amplitude of ≈ 10 μT in the $0.5 \leqslant T \leqslant 6$ K range. For lower temperatures (i.e., 18 mK $\leqslant T \leqslant 4$ K), a dilution refrigerator was used with the same excitation amplitude and frequencies between 13 and 1113 Hz. The electrical resistivity was measured using a four-probe dc method in the temperature range from 0.5 K up to room temperature. Specific heat $C_P(T)$ measurements on samples of about 1 g were performed in a semiadiabatic calorimeter at temperatures ranging from 0.5 up to 20 K using a heat pulse technique. Thermal expansion was measured along three perpendicular directions of polycrystals of rectangular shape α_i with the aid of an ultrahigh-resolution capacitive dilatometer. The volume expansion coefficient $\beta(T)=(1/V)dV/dT$ is obtained from the sum of the linear expansion coefficients, $\beta=\alpha_1+\alpha_2+\alpha_3$.

A. High-temperature results

As mentioned before, the cell volume decreases continuously with increasing Rh content and the measurements on intermediate concentrations allow us to better establish the deviation from Vegard's law at $x_V=0.75$, as shown in Fig. 1. Because of the anisotropic crystalline structure of CePd$_{1-x}$Rh$_x$, we have analyzed the x dependence on each crystalline parameter. In the inset of Fig. 1, one observes that
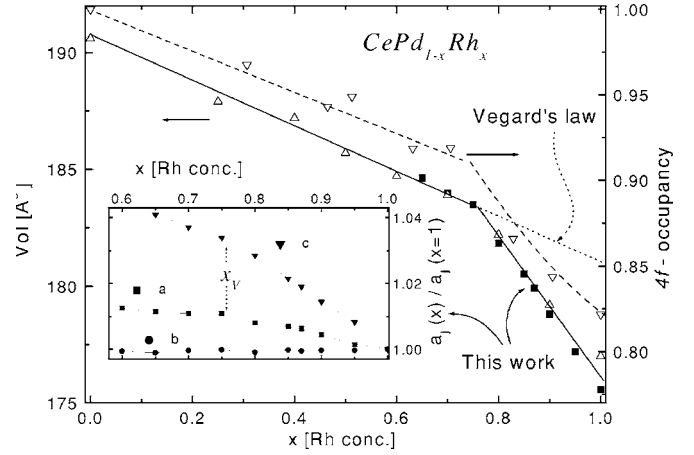

FIG. 1. Concentration dependence of the unit cell volume compared with data from Ref. 16. A clear deviation from Vegard's law occurs at $x_V \approx 0.75$ at the onset of the valence instability, where L_{III}-XAS spectroscopy also indicates a stronger decrease of 4f occupancy (Ref. 16). Inset: normalized variation of each lattice parameter (a_j), showing the crystalline anisotropy of this system.

the change of slope at $x_V=0.75$ occurs on a and c directions, while b remains practically unchanged. In order to confirm that such a deviation from Vegard's law corresponds to the onset of the valence instability, we include in Fig. 1 the L_{III}-XAS results from Ref. 16. These results coincide with the x_V determination as the concentration for the onset of the 4f occupancy decreases.

dc susceptibility (χ_{dc}), measurements under an applied magnetic field of $B=0.1$ T, were carried out on samples within the $0.6 \leqslant x \leqslant 1$ concentration range. The temperature dependence between 2 K and room temperature is depicted in Fig. 2 as $\chi_{dc}^{-1}(T)$. The high-temperature ($T > 100$ K) dependence of samples $0.65 \leqslant x \leqslant 0.87$ can be described by a typical Curie-Weiss law $\chi=C_c/(T-\theta_P)$, with a crystal field and a Kondo induced negative θ_P despite the F-GS (see inset of Fig. 2). Beyond the critical concentration, the system shows the features of a growing valence instability which dominates the CeRh (cf. $x=1$) signal, with a broad maximum centered at ≈ 240 K (not shown). As it occurs in systems undergoing a magnetic to mixed-valence transition, molecular and crystalline electron field (CEF) effects are overcome by the Kondo effect. For that case, a $\chi=C_c/(T+2T_K)$ expression was proposed,[21] where T_K is the Kondo temperature reflecting the J_K increase since $T_K \propto 1/\delta J_K$.[12]

CEF can be observed in $x=0.70$ with $\chi_{dc}(T)$ plotted as a function of temperature in Fig. 3 in a double logarithmic representation. To evaluate the energy of the first excited level (Δ_{CF}), we used a simplified formula applicable to the low-temperature range (i.e., $T < \Delta_{CF}$):

$$\chi(T)_{CF} = [\mu_{GS}^2 + \mu_{CF}^2 \exp(-\Delta_{CF}/T)]/(ZT), \quad (1)$$

where μ_{GS} (μ_{CF}) is the ground (excited) state effective moment and Z is the partition function. Using this simple equation, we obtain $\Delta_{CF} \approx 70$ K and the respective effective moments: $\mu_{GS} \approx 1.5\mu_B$ and $\mu_{CF} \approx 2.8\mu_B$ (see continuous curve on $x=0.70$ in Fig. 3). The strong increase of the χ_{dc} below
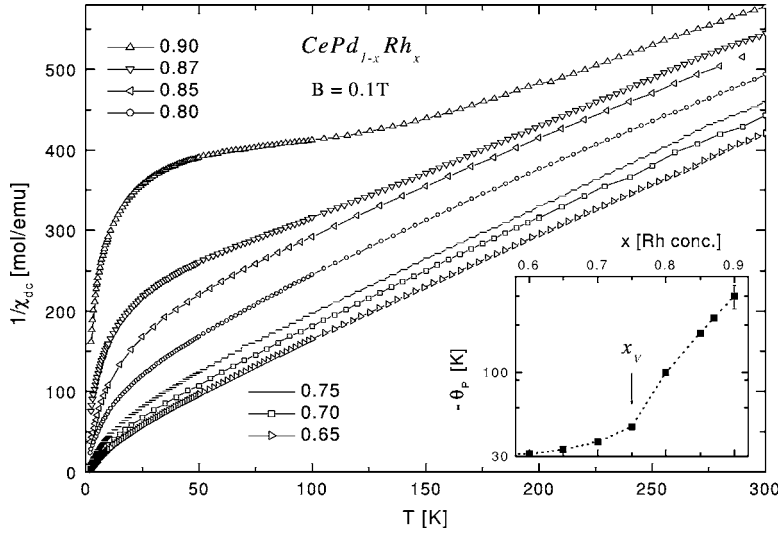
FIG. 2. Inverse dc susceptibility as a function of temperature showing the increasing hybridization effects for $x > 0.75$. Inset: concentration dependence of the Curie-Weiss temperature θ_p extrapolated from $T \geq 100$ K (≥ 200 K for $x=0.90$) on a logarithmic scale.

4 K is due to the onset of ferromagnetic correlations. The progressive weakening of $\mu_{GS}(x)$ evaluated around 2 K is depicted in the inset of Fig. 3. The μ_{GS} points between $0.70 < x < 0.80$ extrapolate to zero at $x \approx 0.90$, whereas the deviation from such extrapolation for $x \geq 0.90$ can be related to remanent low-energy excitations observed in C_m/T measurements to be discussed below.

On the nonmagnetic limit, CeRh shows the typical behavior for a mixed-valence (MV) compound plus a power-law increase at low temperature:

$$\chi(T) = \chi_0 + bT^2 + c/T^q. \qquad (2)$$

The Pauli-type contribution is $\chi_0 = 0.46 \times 10^{-3}$ emu/mol and the bT^2 dependence reflects the presence of spin fluctuations, with $b = 0.12 \times 10^{-3}$ emu/mol K^2. The increase of $\chi(T)$ below about 30 K indicates a reminiscence of magnetic moments even at the CeRh limit. This magnetic contribution cannot be attributed to magnetic impurities because its temperature dependence $c/T^q \propto T^{-0.45}$ does not correspond to a Curie-Weiss law. Furthermore, M vs B measurements at $T = 2$ K and up to $B = 5$ T (not shown) indicate that only a

small magnetic contribution, which saturates at $B \approx 3$ T, is due to impurities. For this compound, the Wilson ratio $R = (\pi k_B / \mu_{eff})^2 \chi_0 / \gamma_0$ corresponds to the expected value $R = 1 + 1/2J = 1.2$ for a MV (i.e., sixfold degenerated) ground state.

The electrical resistivity (ρ) measured up to room temperature in samples with $0.80 \leq x \leq 1$ Rh concentration is displayed in Fig. 4, once normalized to their respective values at room temperature. Two features characterize $\rho(T)$; one is the rapid increase of the hybridization effect on the high-temperature electronic scattering and the other the drastic drop of the residual resistivity (ρ_0) as $x \rightarrow 1$. The former is concomitant with the increase of θ_P ($\propto T_K$) in that concentration range. In the case of $x = 0.80$, a $\rho(T)$ upturn occurs below 10 K (see upper inset in Fig. 4). Such an electronic scattering arises nearly two decades above the χ'_{ac} cusp and thermal expansion minimum (at $T_C = 0.25$ K) and is likely related to the Kondo-type scattering. The lower inset in Fig. 4 shows the $\Delta\rho \propto T^2$ dependence up to ≈ 40 K in pure CeRh. The weak upturn at a very low temperature can be attributed to the moments which are not fully screened by the Kondo effect at that temperature.
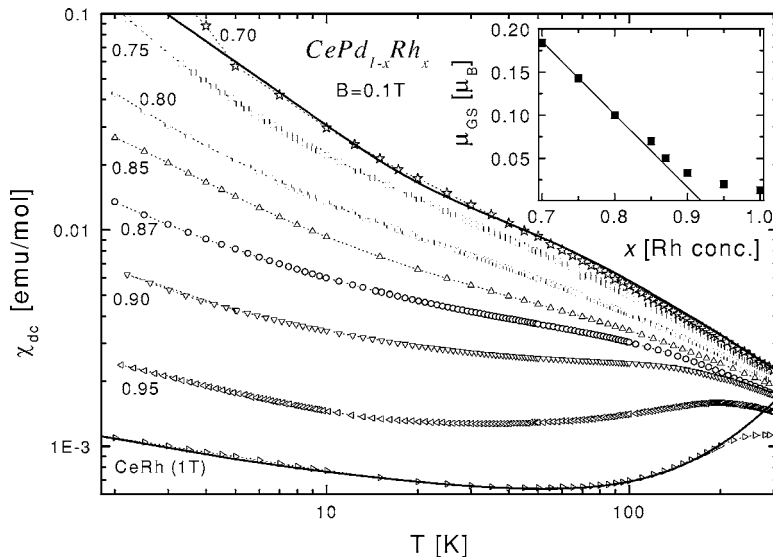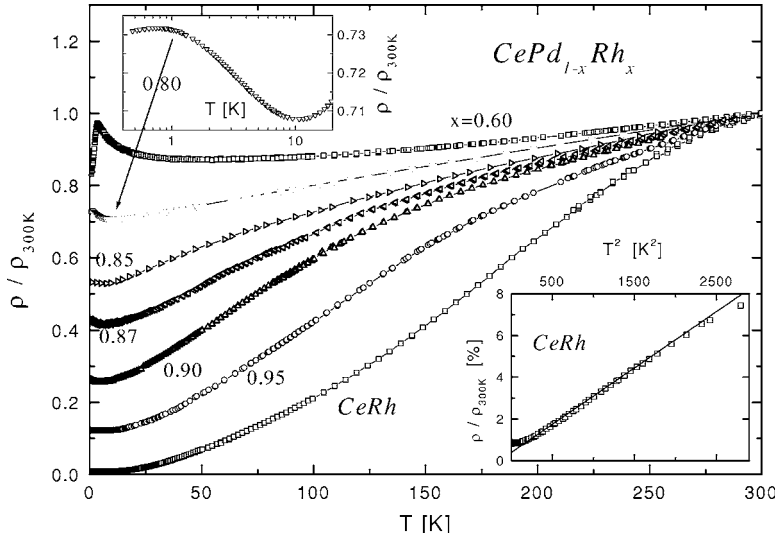

FIG. 3. Temperature dependence of dc susceptibility in a double logarithmic representation showing the effect of hybridization on the excited CEF levels at high temperature and the weakening of the effective moments at low temperature (see the inset). Continuous curves are fits for $x=0.70$ and $x=1$ data using Eqs. (1) and (2), respectively.

FIG. 4. Electrical resistivity normalized at room temperature showing the rapid decrease of the low-temperature scattering beyond x_{cr} and the increase of hybridization effect. Upper inset: detail of the raising magnetic scattering in the $x=0.80$ sample. Lower inset: detail of the $\rho \propto T^2$ dependence of CeRh up to 40 K and the slight upturn below 15 K.

B. Low-temperature results

In order to determine $T_C(x)$ below the lowest value previously reported [T_C=3 K (Ref. 17)], we have performed two sets of χ_{ac} measurements, one down to 0.5 K in a He^3 cryostat and the other down to 20 mK in a dilution refrigerator. The details of the lower-temperature χ_{ac} measurements will be presented and discussed elsewhere. Here, we use a preliminary analysis of these data in order to complete the magnetic phase diagram. The F-phase boundary was traced following the temperature of the maximum of the inductive signal $\chi'_{ac}(T)$ in the $0.60 \leq x \leq 0.87$ samples. These results are presented in Fig. 5 after normalizing the measured signals, with their values at 5 K, and the respective maxima. The sharpness of the anomaly also indicates that eventual atomic disorder introduced by Pd/Rh substitution does not affect the F-transition, which keeps its shape down to the critical concentration (x_{cr}). The difference in the $\chi_{ac}(T)$ curves for $x=0.75$ between the He^3 data and the He^3/He^4 fridge data is

likely due to slight different in the composition of difference pieces of the same large sample and in the frequency of the excitation signal (1.28 kHz and 113 Hz, respectively).

The electronic contribution to the specific heat (C_{el}) was obtained by subtracting the phonon contribution (C_{ph}) from measured values (C_P): $C_{el}=C_P-C_{ph}$. The stoichiometric compound LaRh was taken as the reference for the C_{ph} determination. Figure 6 collects the C_{el}/T results. Though the specific heat magnetic anomaly (C_m) dominates C_{el} in the F-region, upon increasing x, a Fermi liquid (FL) contribution $\gamma(x)$ arising from the MV component becomes important for high Rh concentration. This contribution is accounted for as $C_{el}/T=C_m/T+\gamma$. It can be seen in Fig. 6 that sample $x=0.50$ still shows a sharp transition which broadens for $x \geq 0.60$ (i.e., for $x \geq x^*$). However, the maximum of C_{el}/T stops decreasing and becomes nearly constant for the $x=0.60$, 0.65, and 0.70 samples, as it was observed in other Ce-systems tuned to their quantum critical points (QCPs).[22] Beyond x_{cr}, the γ component tends to dominate the total contribution, and for samples $x=0.90$, 0.95, and 1, the FL contribution is found to be γ=0.047, 0.028, and
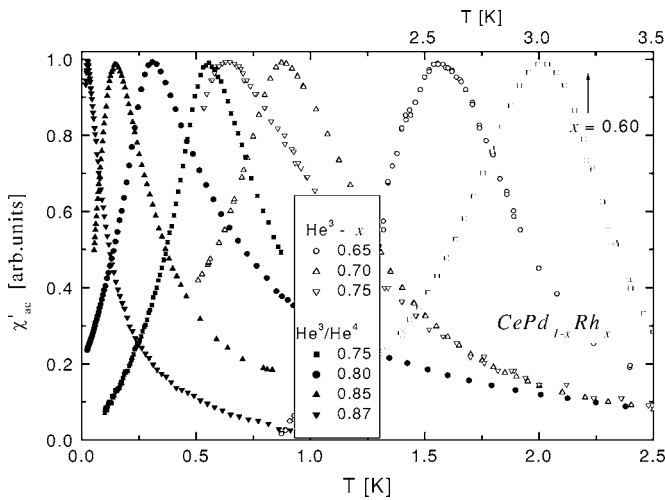

FIG. 5. Inductive signal of ac susceptibility χ'_{ac} normalized at their respective maximum values. For clarity, the temperature dependence of sample $x=0.60$ (only) is depicted on the upper abscissa of the figure.
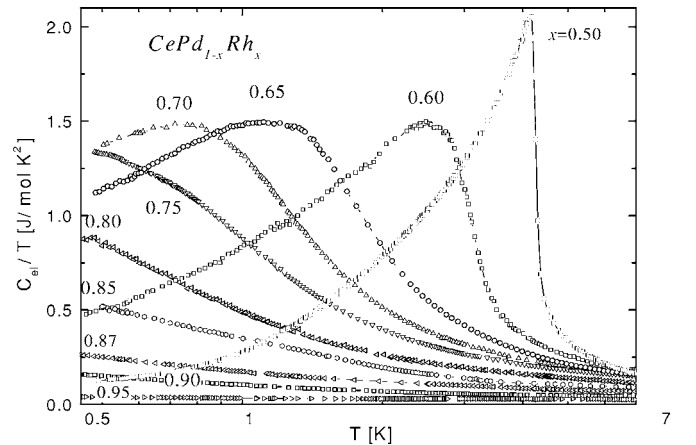

FIG. 6. Total electronic contribution to the specific heat divided by temperature as a function of temperature in a logarithmic scale for samples around the critical region.
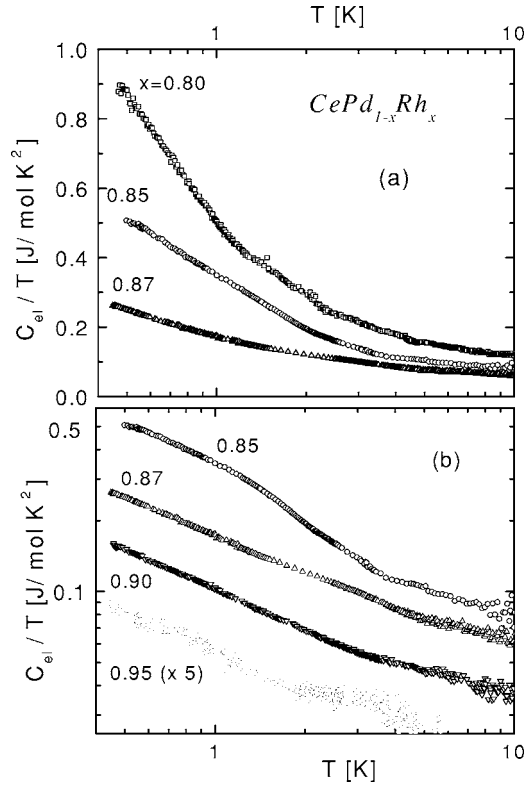
FIG. 7. (a) Specific heat plotted as C_{el}/T vs $\ln T$ showing the logarithmic T dependence at low temperature for $x < x_{cr}$. (b) Double logarithmic representation showing the power-law T dependence close to and beyond the critical concentration. For sample $x=0.95$, the $\gamma=0.028$ J/mol K^2 contribution was subtracted (see text). Note that the data from samples $x=0.85$ and 0.87 are also included for comparison in panels (b) and (a), respectively.

0.017 J/mol K^2, respectively. This type of contribution was observed in many Ce-systems at the onset of their valence instabilities.[13]

A detailed analysis on the temperature dependence of $C_{el}(T)/T$ around x_{cr} is made in Fig. 7. There, a logarithmic temperature dependence is observed for $x=0.80$ and 0.85 samples [see Fig. 7(a)], whereas those with $x=0.87$, 0.90, and 0.95 show a power-law T dependence as proven by the double logarithmic representation in Fig. 7(b). These results are described by a $C_m/T = AT^{-q}$ formula with the exponent $q=0.54\pm0.01$ and $A=0.173$, 0.102, and 0.012 J/mol K^{2-q}, respectively. In the case of sample $x=0.95$, the $\gamma(x)$ contribution was subtracted since it becomes dominant at this Rh concentration.

Thermal expansion measurements performed down to $T \approx 0.1$ K on samples $0.80 \leq x \leq 0.90$ are shown in Fig. 8. The magnetic transition in the $x=0.80$ alloy is clearly identified by a minimum at 0.25 K, coincident with the $\chi'(T)$ measurements. Notable is the change of sign of β between $x=0.80$ and $x=0.85$. Nevertheless, it has to be mentioned that in the last sample, there is still a positive contribution observed in one of the measured directions. Such an anisotropic expansion is certainly related to the intrinsic crystalline anisotropy. A detailed analysis of the non-Fermi liquid behavior of $\beta(T)$ will be presented elsewhere and will be compared with that
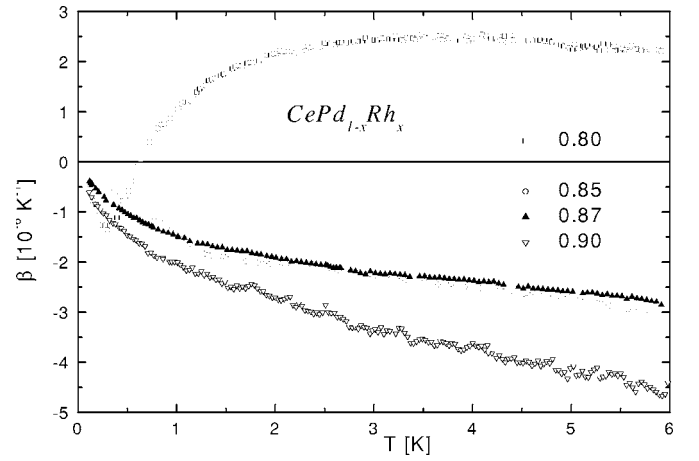

FIG. 8. Thermal expansion measurements showing T_C at 0.25 K for $x=0.80$ and the sudden change of sign between $x=0.80$ and $x=0.85$.

of $C_m(T)$. Like in specific heat measurements, the $\beta(T)$ dependence observed in $x=0.87$ and 0.90 samples is very well described by a power law with a similar exponent q.

III. DISCUSSION

The competition between the vanishing F-order and the growing Kondo screening upon Rh increase is visualized in the magnetic phase diagram in Fig. 9. There, one sees that instead of a continuous negative curvature of $T_C(x)$, an inflection in the phase boundary occurs at $x^* \approx 0.65$. The characteristic of this concentration is that $T_K(x)$ [considered $\propto \theta_P(x)$ (Ref. 21)] starts to strongly increase, as shown on the right side of Fig. 9 in a logarithmic scale. Though the Doni-
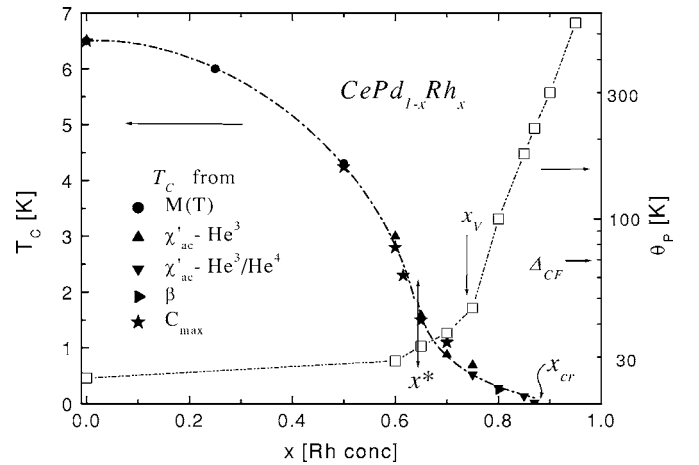
FIG. 9. Magnetic phase diagram for the full concentration range, extracted from magnetic (M, χ'_{ac}) and thermal ($\beta, C_m/T|_{max}$) properties. x^* marks the inflection of the $T_C(x)$ curvature, x_V the onset of the valence instability, and x_{cr} the critical point. The concentration dependence of the Curie-Weiss temperature is included for comparison in a logarithmic scale (on the right axis) to show its rapid increase for $x > x_v$. Δ_{CF} indicates the estimated first CEF splitting. Dash-dot lines are guides to the eyes.

ach model includes both magnetic and Kondo interactions, no reference to a change of curvature is done for the $T_C(x)$ dependence before it vanishes. In order to discuss this behavior, we have to take into account that two effects occur at similar concentrations, as indicated by high- and low-temperature measurements. One concerns the valence instability, indicated by the deviation from Vegard's law and the $4f$ occupation reduction at $x \geqslant x_v$, and the other the presence of the critical point at higher concentration, i.e., $x_{cr} \approx 0.87$. Though this peculiar situation was already observed in other Ce-systems,[13] it was never studied in detail before. In fact, the present investigation demonstrates that the previous $T_C \rightarrow 0$ extrapolation to $x \approx 0.65$ (Ref. [16]) did not account for the change of curvature occurring at $x^* = 0.60$ that originates an extended "tail" in $T_C(x)$ at low temperatures.

Besides the change of curvature, there are other clear indications for significant modifications in the GS properties between x^* and x_{cr}. As mentioned before, the well defined $C_m/T(T_C)$ jump at $x = 0.50$ broadens for $x = 0.60$, keeping a similar relative width and the same maximum value up to $x = 0.70$. Since no sudden changes in the atomic order are expected between $x = 0.50$ and 0.60, this modification can be related to the changes in the magnetic interactions occurring near x^*. At higher Rh concentration (cf. 0.80), the $C_m/T(T)$ dependence becomes logarithmic, in agreement with theoretical predictions for three-dimensional itinerant ferromagnets.[23] Coincidentally, the χ_{ac} maximum starts to show frequency (w) dependence for $x \geqslant 0.70$. These features are usually associated with atomic disorder in diluted systems. However, due to the *lattice* character of the magnetic atoms and the similar atomic size of Ce-ligands (cf. Pd and Rh), a sudden increase of disorder between $x = 0.60$ and 0.70 is unlikely. Nevertheless, in an ample concept of disorder, the presence of random distribution of interactions competing in certain ranges of energy has to be taken into account. Magnetic (J_R) and Kondo (J_K) interactions, favored by the respective Pd and Rh Ce-neighbors with random spatial distribution, are expected to build up an inhomogeneous environment for those parameters. In such a scenario, no more long-range F-order is expected. To highlight the difference in the behavior at the transition between $x < x^*$ and $x > x^*$, in the latter region the transition temperature as determined by the peak in $\chi'_{ac}(T)$ is labeled as $T_C^*(x)$.

It was shown that random hybridization $[\propto J_K(x)]$ leads to a finite probability of very small T_K values (T_K^L) and to a non-Fermi-liquid behavior.[24] This may explain the fact that a magnetic character of the GS may coexist with a strong increase of $T_K(x > x_V)$. On the other hand, spin disordered systems close to their QCPs were described as Griffiths phases due to the possible formation of nonpercolating magnetic clusters.[25] Since this scenario predicts a power-law $C_m(T)$ dependence, for our case it only applies to the $x > x_{cr}$ region. A more realistic description can be done, accounting for an inhomogeneous distribution of each Ce environment, where $J_R(x)$ and $J_K(x)$ act simultaneously.[26]

The strong anisotropy of this system is also expected to play a role in the coexistence between a magnetic GS and the strongly hybridized excited CEF levels. The orthogonal character of the CEF level wave functions leads to the possibility
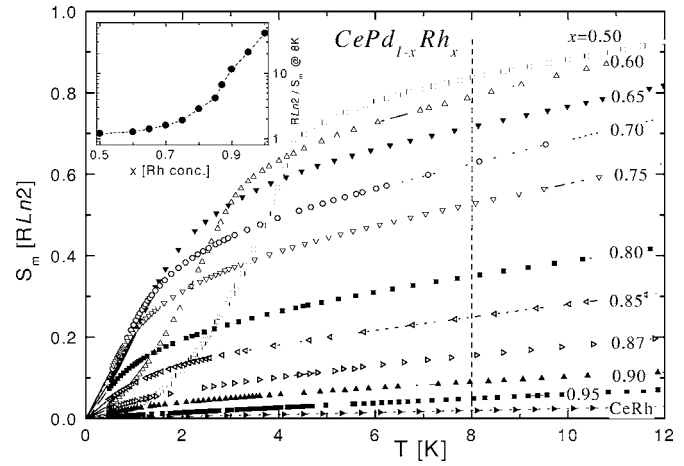

FIG. 10. Thermal entropy gain for all studied samples, normalized to $R \ln 2$. Inset: inverse of entropy at a fixed temperature (8 K) as a function of concentration (see the text).

of different local and conduction spin coupling intensities due to their different mixing matrix elements. Such a situation becomes sensitive when $T_K \approx \Delta_{CF}$ since the broadening of the excited CEF levels increases their influence on the low energy range.

The actual hybridization effect on the low-lying levels (cf. T_K^L) can be qualitatively evaluated through a low temperature property such as the magnetic entropy $[S_m(x,T)]$. Taking advantage of the fact that $S_m \propto 1/T_K$,[27] one can obtain $T_K^L(x)$ from the measured S_m at a fixed temperature. In this case, we have extracted S_m at $T = 8$ K from the $S_m(T)$ data shown in Fig. 10 and have computed the $R \ln 2/S_m(x)$ values as depicted in the inset of Fig. 10. Though on the Rh rich side its tendency is similar to the extracted form $\theta_P(x)$, a deviation between those parameters is observed between x_V and x_{cr} since GS and CEF excited levels are differently hybridized in that region. A further increase of $J_K(x)$ leads to the collapse of the CEF effect, and the sixfold degenerated Hund's rule GS takes over at the MV limit.

The change of sign in the thermal expansion indicates that the volume behaves completely different on both sides of the critical concentration. Upon heating, sample $x = 0.80$ first contracts to undergo the magnetic transition and then rapidly expands. On the contrary, for $x \geqslant 0.85$, the volume continuously contracts (at least up to 6 K). The negative sign of $\beta(T)$ for $x \geqslant 0.85$ is quite surprising because in that concentration range, the MV regime becomes dominant. In fact, the well-known Ce-MV compounds show a positive $\beta(T)$ coefficient [e.g., $CeSn_3$ (Ref. [28])] because the main energy scale, related to T_K, increases under pressure. However, since this observation corresponds to the low-temperature range (i.e., up to 6 K $\ll T_K$), it only involves the low-energy excitations of the system, where a diverging C_m/T component is still present. Taking advantage of the fact that the linear thermal expansion of each sample was measured in three perpendicular directions, further information about anisotropic effects of this system can be extracted. Notably, only in one direction is $\alpha(T)$ positive (arbitrarily labeled as α_1) and becomes zero at $x = 0.87$, whereas the others (α_2 and α_3) show an increasing
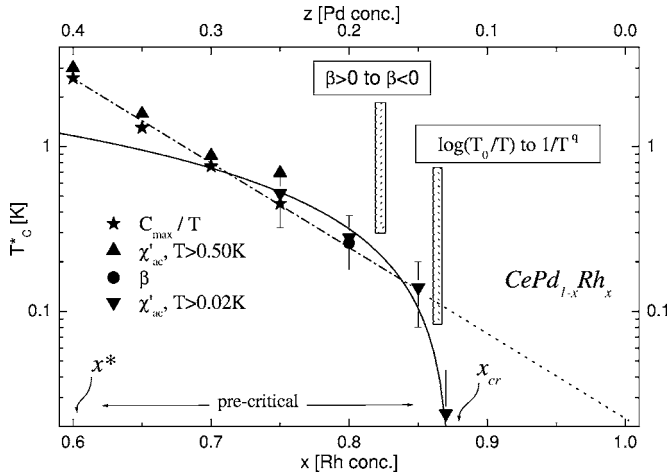
FIG. 11. $T_C^*(x)$ dependence at the precritical concentration showing logarithmic decrease and sudden disappearance of the $\chi_{ac}'(T)$ cusp. The change of thermal properties is indicated around the critical concentration.

negative temperature dependence. Further measurements on single crystals are certainly required to relate this anisotropic behavior to the actual crystalline axis, see Ref. 29.

In Fig. 11, we show a detailed $T_C^*(x \geq 0.60)$ dependence obtained from the different techniques, notably χ_{ac}' at very low temperatures, depicted in a logarithmic scale. The positive curved tail, already presented in the phase diagram of Fig. 9, can be described by a simple function $T_C^*(z) = (0.022 \text{ K}) \times e^{12z}$, where $z = 1 - x$ corresponds to Pd concentration. This permutation of the concentration parameter dependence is not a minor detail because it indicates that the $T_C^*(z)$ evolution refers to a *smeared* phase transition.[30] This is in agreement with the remanent low-temperature contribution to C_m/T observed on that side of the phase diagram. Since this description is valid for $z > 0.13$, it suggests that some type of *percolation* between magnetic *rare* regions[2] is needed to produce the cusp detected by χ_{ac}. Such a percolation threshold is in agreement with the onset of the power-law dependence of C_m/T. As mentioned before, the formation of Griffiths phases requires the existence of nonpercolating clusters that occur for $x > 0.87$. The fact that the T_C^* variation can be simply described as a function of z suggests that the physics in that region is governed by a sort of "virtual" critical point lying beyond the CeRh limit. For comparison, we have included in Fig. 11 a linear $T_C^*(x \geq 0.70)$ dependence (see continuous line) because it also represents a good description for this phase boundary if the $x = 0.87$ point at $T_C^* = 27$ mK is included.

Within this context, the phase diagram presents two distinct regions represented by the T_C canonical boundary and the T_C^* curve. On the former region (cf. $0 \leq x \leq x^*$), the $T_C(x)$ phase boundary (6 K $\geq T_C(x) > 2$ K) points to the early critical concentration proposed at $x \approx 0.65$.[17] Beyond x^* (i.e., below about 2 K), another type of criticality dominates the scenario according to the drastic changes in the low-temperature properties. The question arises whether this threshold is governed by concentration (i.e., chemical potential) or by the exhausting thermal fluctuations overcome by quantum fluc-

tuations. Such a *thermal* threshold is not an arbitrary proposition since other well-known AF-Ce systems show similar changes in their magnetic phase boundaries at that temperature (cf. thermal energy). Some of them even occur close to a first-order transition, e.g., CeIn$_{3-x}$Sn$_x$ with $x^* \approx 0.40$, where $T_N = 2$ K (Ref. 22) and CeCu$_2$(Si$_{1-y}$Ge$_y$)$_2$ with $y^* = 0.25$ K and the same $T_N = 2$ K value.[31]

Another important observation in this region is the frequency (w) dependence of the χ_{ac}' cusp. Such a dependence is only observed for $x \geq 0.70$. Here, the question arises whether it is due to a canonical spin-glass behavior or to fluctuations related to the QCP. Since a $C_m/T \propto -\log(T/T_0)$ dependence is predicted for a non-Fermi-liquid behavior (instead of the $\propto 1/T^2$ for a spin glass), quantum critical fluctuations are expected to be mainly responsible for such $\chi_{ac}'(w)$ dependence.[32] Nevertheless, other hallmarks of spin-glass GS, such as the difference between zero-field cooling and field cooling and the time dependence of the χ_{ac}' response under field suppression, have to be explored.

IV. CONCLUSIONS

The phase diagram of F-CePd$_{1-x}$Rh$_x$ was traced between $T_{C,x=0} = 6$ K and $T_{C,x=0.87}^* \approx 20$ mK. Three characteristic concentrations were identified: $x^* \approx 0.65$, $x_V \approx 0.75$, and $x_{cr} \approx 0.87$. The former marks the crossover from a classical phase boundary (with a negative curvature) into a positive curved "tail" which drops at $x_{cr} = 0.87$. In that region, a frequency dependence of the χ_{ac}' cusp is also detected.

Independently of the magnetic GS, a deviation from Vegard's law occurs at x_V, indicating the onset of the valence instability. Beyond that concentration, $T_K(x)$ increases exponentially. Unlike typical AF systems, where $x_V > x_{cr}$, this ferromagnet has its critical concentration beyond the onset of the valence instability, i.e., $x_V < x_{cr}$. Such a characteristic inhibits the appearance of HF behavior because at that concentration, J_K is already largely developed, leading to the broadening of the quasiparticle band with the consequent reduction of their effective mass. Besides this $\gamma(x)$ decrease, there is a remanence of low-lying magnetic excitations accounted for by the $C_m/T \propto 1/T^q$ contribution. Such a coexistence of magnetism with highly hybridized quasiparticles occurs in an inhomogeneous distribution of J_R and J_K couplings produced by the random distribution of Pd and Rh Ce-ligands.

The coexistence of different behaviors observed at high and low temperatures may be related to different degrees of hybridization between ground and excited CEF levels. The possibility of such a scenario is suggested by the strong anisotropic character of this system, clearly manifested in the crystalline parameters and thermal expansion properties.

The outstanding findings around x_{cr} are the change of $C_m/T(T)$ dependence from logarithmic to power law, occurring close to the change of sign of $\beta(T)$. Though in the pre-critical ($x^* < x < x_{cr}$) region, the logarithmic $C_m/T(T)$ dependence is in agreement with the theoretical predictions for three-dimensional itinerant ferromagnets, its transformation to a power law indicates that the formation of "rare" regions can play an important role in this behavior. The coexistence

of ferromagnetic and valence fluctuations results in a $\rho(T)$ upturn at low temperature, providing evidence for an electronic scattering with low-lying excitations.

A better understanding of the phase diagram can be achieved by recognizing two different regions: one with long-range F-order, which extrapolates $T_C(x) \to 0$ at ≈ 0.65, and the other (below about 2 K) extrapolating $T_C^*(x)$ beyond the CeRh limit. Altogether, $CePd_{1-x}Rh_x$ has proven to be an exemplary system for studying the influence of doping on the quantum criticality in a ferromagnetic environment and a number of physical properties are revealed by covering more than two and a half decades of temperature.

ACKNOWLEDGMENTS

[1] See, e.g., Proceedings of SCES'04 [Physica B **359-361** (2005)] Proceedings of SCES'05 [Physica B **378-380** (2006)].

[2] T. Vojta, Ann. Phys. **9**, 403 (2000).

[3] P. Coleman and A. Schofield, Nature (London) **433**, 225 (2005).

[4] G. R. Stewart, Rev. Mod. Phys. **73**, 797 (2001).

[5] See, for example, S. M. Evans, A. K. Bhattacharjee, and B. Coqblin, Physica B **171**, 293 (1991).

[6] M. Uhlarz, C. Pfleiderer, and S. M. Hayden, Phys. Rev. Lett. **93**, 256404 (2004).

[7] T. R. Kirkpatrick and D. Belitz, Phys. Rev. B **67**, 024419 (2003).

[8] J. G. Sereni, in *Handbook for Physics and Chemistry of Rare Earths*, edited by K. A. Gschneidner, Jr. and L. Eyring (Elsevier Science B. V, New York, 1991), Vol. 15, Chap. 98.

[9] S. Süllow, M. C. Aronson, B. D. Rainford, and P. Haen, Phys. Rev. Lett. **82**, 2963 (1999).

[10] T. Burghardt, A. Eichler, S. Sülow, and J. A. Mydosh, Physica B **259-261**, 99 (1999).

[11] J. Larreaj, M. B. Fontes, A. D. Alvarenga, E. M. Baggio-Saitovich, T. Burghardt, A. Eichler, and M. A. Continentino, Phys. Rev. B **72**, 035129 (2005).

[12] S. Doniach, Physica B & C **91B**, 231 (1977); M. Lavagna, C. Lacroix, and M. Cyrot, Phys. Lett. **90A**, 210 (1982).

[13] J. G. Sereni, Physica B **215**, 273 (1995), and references therein.

[14] B. Coqblin, J. Arispe, J. R. Iglesias, C. Lacroix, and K. Le Hur, J. Phys. Soc. Jpn. **65**, 64 (1996).

[15] T. Vojta, Phys. Rev. Lett. **90**, 107202 (2003).

[16] J. P. Kappler, M. J. Besnus, A. Herr, A. Meyer, and J. Sereni, Physica B **171**, 346 (1991).

[17] J. G. Sereni, E. Beaurepaire, and J. P. Kappler, Phys. Rev. B **48**, 3747 (1993).

[18] J. G. Sereni, R. Küchler, and C. Geibel, Physica B **359-361**, 41 (2005).

[19] J. G. Sereni, J. Phys. Soc. Jpn. **70**, 2139 (2001).

[20] D. Hohnke and E. Parthé, Acta Crystallogr. **20**, 572 (1966).

[21] H. R. Krishna-murthy, K. G. Wilson, and J. W. Wilkins, Phys. Rev. Lett. **35**, 1101 (1975).

[22] See, for example, P. Pedrazzini, M. G.-Berisso, N. C.-Canales, M. Deppe, C. Geibel, and J. G. Sereni, Eur. Phys. J. B **38**, 445 (2004).

[23] L. B. Ioffe and A. J. Millis, Phys. Rev. B **51**, 16151 (1995).

[24] E. Miranda, V. Dobrosavljevic, and G. Kotliar, Phys. Rev. Lett. **78**, 290 (1997).

[25] A. H. CastroNeto, G. Castilla, and B. A. Jones, Phys. Rev. Lett. **81**, 3531 (1998).

[26] A. M. Lobos, A. A. Aligia, and J. G. Sereni, Eur. Phys. J. B **41**, 289 (2004).

[27] H.-U. Desgranges and K. D. Schotte, Phys. Lett. **91A**, 240 (1982).

[28] See, for example, J. G. Sereni, J. Phys. F: Met. Phys. **10**, 2831 (1980).

[29] M. Deppe, P. Pedrazzini, N. Caroca-Canales, C. Geibel, and J. G. Sereni, Physica B **378-380**, 96 (2005).

[30] For a "smeared quantum phase transition" description, see R. Sknepnek and T. Vojta, Phys. Rev. B **69**, 174410 (2004).

[31] O. Stockert, M. Deppe, E. Faulhaber, H. S. Jeevan, R. Schneider, N. Stuesser, C. Geibel, M. Lövanhaupt, and F. Steglich, Physica B **359-361**, 349 (2005).

[32] D. R. Grempel and M. J. Rozenberg, Phys. Rev. B **60**, 4702 (1999).